nature physics

LETTERS

PUBLISHED ONLINE: 2 MAY 2010 | DOI: 10.1038/NPHYS1656

Evidence for a Lifshitz transition in electron-doped iron arsenic superconductors at the onset of superconductivity

Chang Liu[1†], Takeshi Kondo[1†], Rafael M. Fernandes[1], Ari D. Palczewski[1], Eun Deok Mun[1], Ni Ni[1], Alexander N. Thaler[1], Aaron Bostwick[2], Eli Rotenberg[2], Jörg Schmalian[1], Sergey L. Bud'ko[1], Paul C. Canfield[1] and Adam Kaminski[1]*

The iron arsenic high-temperature superconductors[1,2] exhibit particularly rich phase diagrams. In the AE$(Fe_{1-x}T_x)_2As_2$ family (known as '122', with AE being Ca, Sr or Ba and T being a transition metal), the simultaneous structural/magnetic phase transition that occurs at elevated temperature in the undoped material splits and is suppressed by carrier doping[3,4]. A superconducting region appears as likely in the orthorhombic/antiferromagnetic (AFM) state as in the tetragonal/paramagnetic state[3,5,6]. An important question then is what determines the critical doping at which superconductivity emerges, as the AFM order is fully suppressed only close to optimal doping. Here we report evidence from angle-resolved photoemission spectroscopy that marked changes in the Fermi surface coincide with the onset of superconductivity in electron-doped $Ba(Fe_{1-x}Co_x)_2As_2$. The presence of the AFM order leads to a reconstruction of the electronic structure, most significantly the appearance of the petal-like hole pockets at the Fermi level. These hole pockets vanish—that is, undergo a Lifshitz transition[7]—as the cobalt concentration is increased sufficiently to support superconductivity. Superconductivity and magnetism are competing states in this system: when petal-like hole pockets are present, superconductivity is fully suppressed, whereas in their absence the two states can coexist.

Previous studies demonstrated that the presence of the long-range AFM order leads to a substantial reconstruction of the Fermi surface at low temperature in the undoped pnictides[8–14], as well as in the hole-doped $Ba_{1-x}K_xFe_2As_2$ system[15]. Here we report a systematic study of electron-doping effects on the reconstructed Fermi-surface sheets and relate it to the emergence of superconductivity. In Fig. 1a,b we present the Fermi-surface maps of $Ba(Fe_{1-x}Co_x)_2As_2$ at $T = 20$ K for two extreme doping levels: $x = 0$ where AFM order is present and $x = 0.114$ where it is fully suppressed by cobalt doping. In the undoped samples the X-pocket Fermi surface looks like four flower petals—high-intensity peaks are visible along the diagonal $k_{(110)}$ and $k_{(1\bar{1}0)}$ directions. For $x = 0.114$ samples, the X-pocket Fermi surface changes to an oval shape and the peaks along the $k_{(110)}$ direction are absent. In Fig. 1c–j we point out the magnetic origin of this Fermi-surface reconstruction by comparing the X-pocket details to the prediction of a model calculation. We use a five-band tight-binding model (see Supplementary Information) with and without an AFM order. The presence of the AFM order is measured by mean-field order parameters Δ_{AF} and Δ' that represent intra-orbital and inter-orbital magnetic interactions, respectively, and lead to opening of gaps in the AFM state. The observed Lifshitz transition (detailed later) occurs only as a consequence of Δ' and is evidence for the importance of inter-orbital magnetic interactions, which were argued to be essential for spin-fluctuation-induced superconductivity[16]. The comparison shown in Fig. 1 clearly demonstrates that the observed Fermi-surface reconstruction is consistent with the effects of a long-range AFM order and inter-orbital coupling on the electronic structure. In the undoped sample with AFM order, the four Fermi peaks that make up the 'flower petals' appear in both the experimental data and the theoretical calculation, and they are hole-like—increasing the binding energy results in a larger size of the petals in the constant-energy cuts. In the overdoped paramagnetic state, however, these petals are absent in both the experiment and theory. The main X-pocket is electron-like—increasing the binding energy results in smaller pockets. We will use these features to study the effects of doping on the Fermi surface and its relation to superconductivity in electron-doped pnictides.

In Fig. 2 we plot the angle-resolved photoemission spectroscopy (ARPES) Fermi-surface maps at $T = 13$ and 150 K for several different cobalt doping levels obtained with a photon energy of 21.2 eV (He–I line). It is clear that the reconstructed hole pockets are present for $x < 0.034$ at low temperatures and vanish at $T = 150$ K, above the magnetic transition temperature T^*. It is worth noting that the temperature dependence of the Fermi surface is not due to thermal broadening, because the low- and high-temperature data for higher doping levels are very similar. The first and most important observation in Fig. 2 is that the small hole-like pockets vanish from the Fermi level rather rapidly at intermediate doping levels. At low temperature the intensity of those petals starts to decrease at a doping level of $x = 0.024$, and effectively the intensity has vanished by $x = 0.038$. This is due to the fact that the top of the hole bands moves below the Fermi energy, which is a classic signature of a Lifshitz transition[7] (see Fig. 3c), and it coincides with the emergence of superconductivity in the phase diagram. ARPES data consistent with this picture are also taken with a linear polarized synchrotron beam (see Supplementary Information). In Fig. 2b we quantify this transition by plotting the maximum intensity around the X-pocket Fermi surface (from

[1]Ames Laboratory and Department of Physics and Astronomy, Iowa State University, Ames, Iowa 50011, USA, [2]Advanced Light Source, Lawrence Berkeley National Laboratory, Berkeley, California 94720, USA. †These authors contributed equally to this work. *e-mail: kaminski@ameslab.gov.

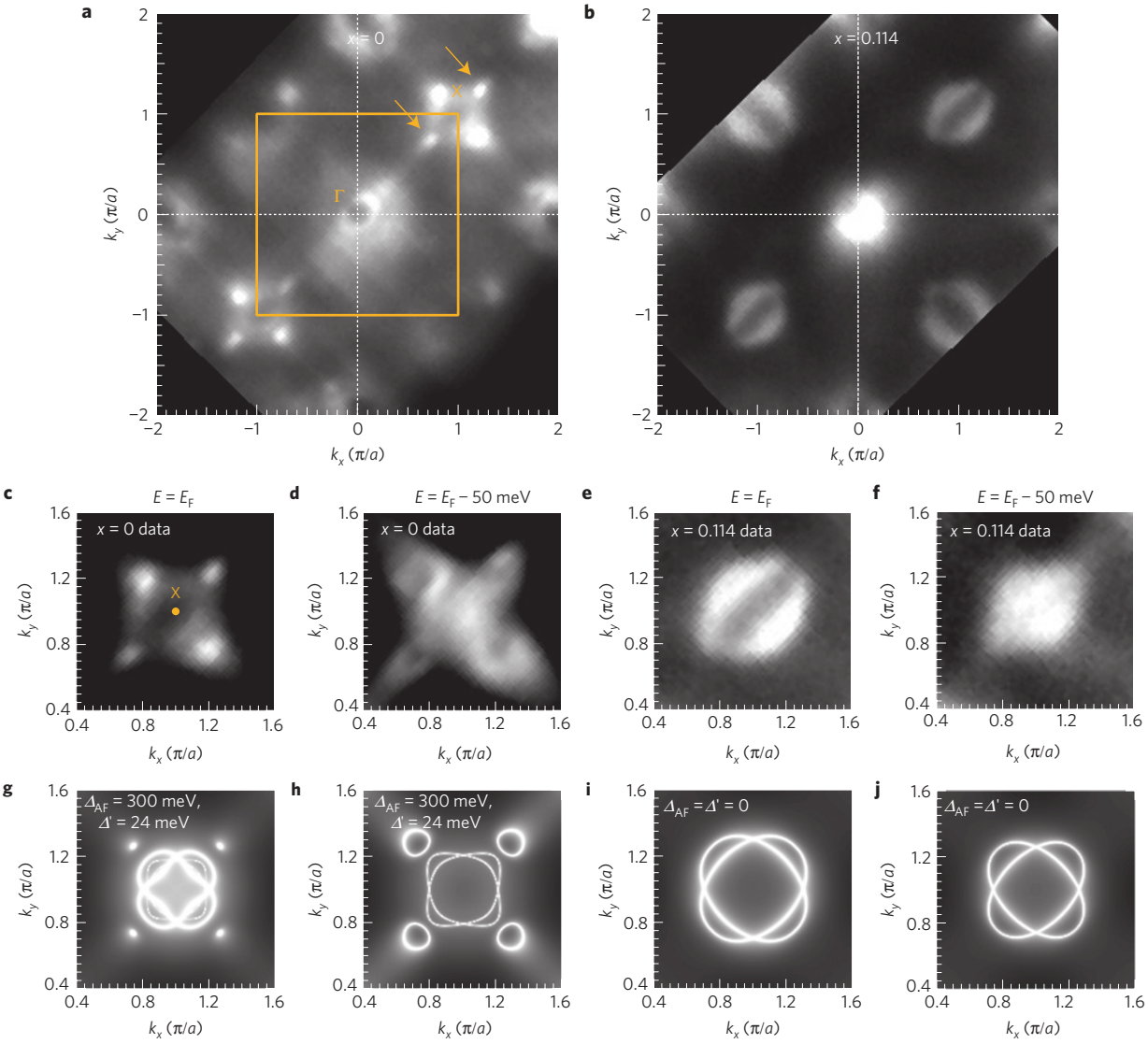

Figure 1 | The Fermi-surface reconstruction and its magnetic origin. a,**b**, Fermi-surface mappings of $Ba(Fe_{1-x}Co_x)_2As_2$—intensity of the photoelectrons integrated over 10 meV about the chemical potential. Data are taken with 105-eV photons in the AFM ($x = 0$) and paramagnetic ($x = 0.114$) phases at $T = 20$ K. The bright areas indicate higher intensity. The orange arrows in **a** emphasize the Fermi peaks along the $k_{(110)}$ direction. **c**–**f**, Expanded ARPES intensity plots in the vicinity of the X-points for two different binding energies indicated at the top of each graph. **g**–**j**, Results of a five-band tight-binding model calculation for the same binding energies. Δ_{AF} is a measure of the AFM order parameter; Δ' is a measure of the inter-orbital coupling strength.

panels in Fig. 2a) as a function of the angle (α) with respect to the $k_{(110)}$ direction. With hole pockets present ($0 < x < 0.024$) there is a strong peak at $\alpha = 0°$. This peak decreases as x changes from 0.024 to 0.034 and vanishes by $x = 0.038$. Beyond this doping these small hole pockets are absent. Neutron scattering experiments[5,17] clearly demonstrate that long-range AFM order coexists and competes with superconductivity beyond $x = 0.04$, and probably extends up to $x \sim 0.06$. Indeed, in ARPES data the reconstruction of the electronic structure is observed up to $x = 0.058$, but only at higher binding energies (see Supplementary Information). As the doping increases beyond $x \sim 0.03$, the small hole pockets disappear and superconductivity can take place even in the AFM state.

In Fig. 2c we focus on the doping evolution of the nesting condition by examining the contours of the X- and Γ-pocket Fermi-surface sheets in the doping region where the petals are absent. For $0.038 < x < 0.073$, both pockets are roughly similar in shape and size, indicating reasonably good nesting conditions. For $x = 0.114$, however, the X-pocket is significantly larger than the Γ-pocket, yet the sample is still superconducting ($T_C = 12.8$ K). Thus, superconductivity can exist in these materials even in the absence of perfect nesting, in contrast to what was previously suggested[18].

Our ARPES results explain the marked changes with doping reported from Hall effect and thermoelectric power (TEP) measurements[19–21]. In Fig. 3a we plot the Hall coefficient R_H as a function of doping at $T = 25$ and 150 K (ref. 19) measured on samples from the same batch as those used for the ARPES measurements. We compare this with the maximum ARPES intensity of the reconstructed Fermi surface at the chemical potential (defined in the caption) for the data from both the helium lamp and the synchrotron, which is a way to quantify the changes in the Fermi-surface topology. The two ARPES data sets are qualitatively consistent with each other. From the helium lamp data, one can observe that not only does the change in the above-defined ARPES intensity correlate with the marked increase in the Hall coefficient, it also coincides with the onset of superconductivity at $0.024 < x < 0.028$. In a similar manner to the Hall coefficient, the TEP (ref. 19) (not shown) changes abruptly with doping between $x = 0.02$ and $x = 0.024$ (right at the onset of the changes in the

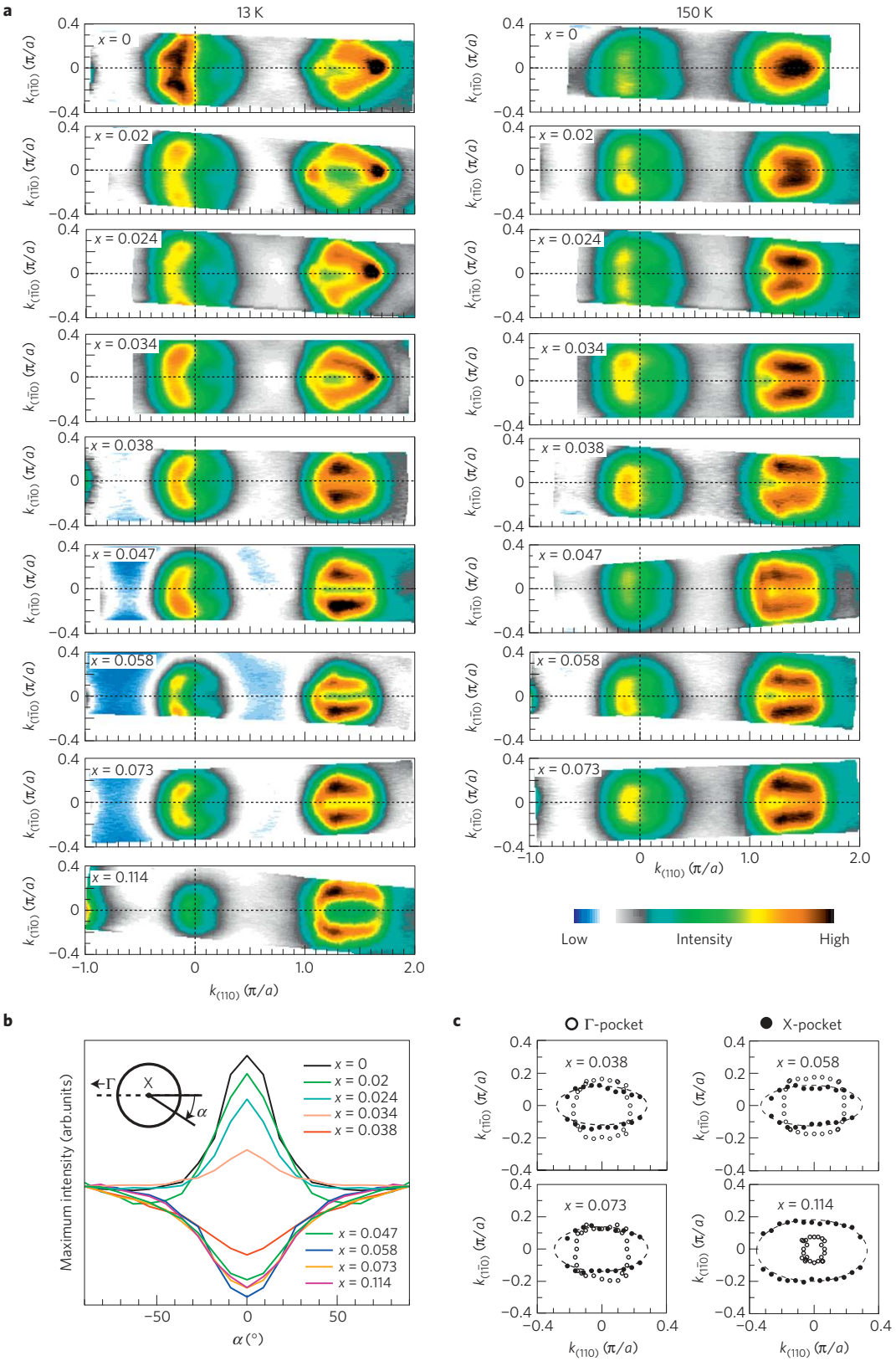

Figure 2 | The vanishing of the marked Fermi-surface reconstruction coincides with the onset of superconductivity. a, Fermi-surface mappings of $Ba(Fe_{1-x}Co_x)_2As_2$ for temperatures $T = 13$ and 150 K measured at various cobalt doping levels. The incident photon energy is 21.2 eV. (Note: the image slice is rotated by 45° with respect to Fig. 1.) **b**, Maximum intensity of electrons around the X-pocket for the low-temperature data, shown as a function of an angle α defined in the inset. The intensities are normalized at $\alpha = 90°$ and symmetrized with respect to $\alpha = 0°$. **c**, Γ- and X-pocket location of the low-temperature data extracted through the peak position of the momentum distribution curves for $0.038 \leq x \leq 0.114$. The X-pocket is shifted to the Γ-pocket by rescaling the $k_{(110)}$ axis through $k' = k - \sqrt{2}$ for easier comparison of their areas.

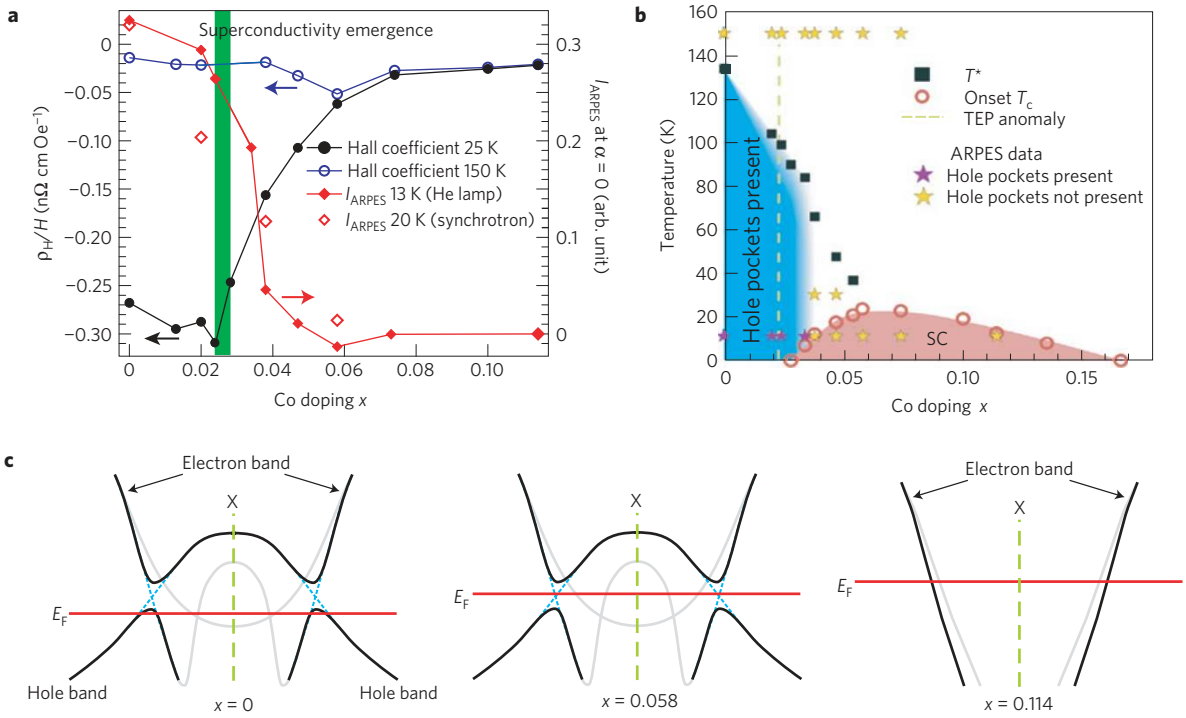

Figure 3 | Summary. a, Left axis: the *a*–*b*-plane Hall coefficient $R_H \equiv \rho_H/H$ versus x of $Ba(Fe_{1-x}Co_x)_2As_2$ with magnetic field $H = 90$ kOe $\| c$, $T = 25$ and 150 K (ref. 19). Right axis: ARPES intensity I_{ARPES} at $\alpha = 0°$ extracted from both helium lamp and synchrotron data, minus I_{ARPES} at $x = 0.114$. **b**, Schematic phase diagram of $Ba(Fe_{1-x}Co_x)_2As_2$ based on ARPES and transport measurements[19]. Both the magnetic transition temperature T^* and the onset temperature of superconductivity are determined by resistivity measurements. **c**, Schematic band dispersion for three different doping levels at the vicinity of the X-point. In the AFM state ($0 < x < 0.058$) the electron bands and hole bands fold back onto each other, and hybridize because of the existence of inter-band coupling. The Lifshitz transition takes place when the tip of a hybridized band sinks below the Fermi level because of increasing electron occupation.

Hall coefficient) for a surprisingly wide range of temperatures ($25\,K < T < 300\,K$). This implies that TEP is much more sensitive to the underlying electronic properties. The Hall effect and TEP measurements together set a finer range for the Lifshitz transition as they reflect the effects of the electronic structure on the macroscopic physical properties of the sample. It is also noteworthy that other electron-doped 122 systems show essentially the same phase diagram as that of the cobalt-doped samples[22,23] and similar changes in Hall coefficient and TEP are also observed (for Cu-doped $BaFe_2As_2$(ref. 22) and for Ni-doped $SrFe_2As_2$ where the onset of the Hall coefficient and TEP anomaly also occurs right at the onset of superconductivity[23]). This suggests that the Lifshitz transition reported here is a general property for the electron-doped 122 systems. It is not clear whether or not this conclusion can be extrapolated to the hole-doped side of the phase diagram. On one hand, assuming a simple rigid band shift, one would expect the petals to be present in the hole-doped 122 system and indeed they were observed by ARPES in $Ba_{1-x}K_xFe_2As_2$ (refs 15,24). On the other hand, the situation in $Ba_{1-x}K_xFe_2As_2$ is significantly complicated by spatial inhomogeneity[24] and evidence from local probes (for example, nuclear magnetic resonance) suggests that AFM and superconductivity are microscopically separated[25,26]. In this case the impact of down folding on the superconducting state is not an issue and superconductivity is suppressed at low hole doping by the emergence of a first-order phase boundary between the two states[27]. The question of why superconductivity is compatible with the petals in the hole-doping regime is an important one and requires further detailed experimental investigation.

We summarize our main findings in Fig. 3b, where we plot the locations of each ARPES spectrum on the x–T phase diagram. Figure 3b shows that the emergence of superconductivity in $Ba(Fe_{1-x}Co_x)_2As_2$ coincides with the disappearance of the reconstructed pieces of the Fermi surface. Our observation explains that the changes in Hall coefficient, namely the rapid increase of R_H, are caused by rapid changes of the Fermi-surface topology with doping. As shown in Fig. 3c, a Lifshitz transition takes place close to the emergence of superconductivity, when the hybridized petal-like hole pockets fill up because of an increase in electron occupation. Long-range magnetic order has a particularly strong impact on the pairing interaction in the case of unconventional superconductivity because of magnetic fluctuations. The pairing interaction resulting from spin fluctuations on the reconstructed Fermi surface is reduced because of the requirement that the quasiparticle-induced spin wave damping vanishes at the ordering vector[28]. In the context of the pnictides, this effect leads to the reduced pairing interaction of the magnetically ordered state because the modified wavefunctions in the magnetically ordered state couple less efficiently to magnetic fluctuations[29]. This effect is strongest for large magnetization with pronounced down folding and demonstrates the sensitivity of an electronic pairing mechanism with respect to an AFM Fermi-surface reconstruction. The finding of the present letter demonstrates that avoiding the Fermi-surface reconstruction may be the key to establishing the superconductivity in electron-doped iron arsenic high-temperature superconductors.

Methods

Single crystals of $Ba(Fe_{1-x}Co_x)_2As_2$ were grown by self-flux using conventional high-temperature solution growth techniques. The doping level x for each sample batch was determined using wavelength dispersive X-ray spectroscopy in a JEOL JXA-8200 electron microprobe; the doping inhomogeneity is kept as low as $\Delta x/x < 7\%$ (ref. 3). Transport and magnetization measurements report a tetragonal to orthorhombic structural transition with a paramagnetic to AFM transition at $T_S \approx T^* \approx 135\,K$ for the undoped ($x = 0$) samples. Increasing the

doping significantly suppresses and splits the two transition temperatures[3–5]; superconductivity appears around $x \sim 0.025$ and a maximum onset T_C of ∼24 K was observed for the $x = 0.058$ samples[3]. The ARPES measurements were carried out at a laboratory-based ARPES system consisting of a Scienta SES2002 electron analyser, GammaData ultraviolet lamp and custom-designed refocusing optics at Ames Laboratory, as well as beamline 7.0.1 of the Advanced Light Source (ALS), Berkeley, California with a Scienta R4000 electron analyser. Vacuum conditions were better than 3×10^{-11} torr. The energy resolution was set at ∼25 meV for Fig. 1 and ∼9 meV for Fig. 2. All samples were cleaved *in situ* yielding mirror-like, clean *a*–*b* surfaces. Cleaved surfaces of all samples were stable for at least 24 h. Results were reproduced at the ALS beamline 7.0.1 as well as Ames Laboratory on several samples. The high symmetry point X is defined to be $(\pm\pi/a, \pm\pi/a(b), 0)$ with the k_x and k_y axes along the Fe–As bonds.

Received 18 September 2009; accepted 11 March 2010; published online 2 May 2010

References

1. Kamihara, Y., Watanabe, T., Hirano, M. & Hosono, H. Iron-based layered superconductor La[$O_{1-x}F_x$]FeAs ($x = 0.05$–0.12) with $T_c = 26$ K. *J. Am. Chem. Soc.* **130,** 3296–3297 (2008).
2. Rotter, M., Tegel, M. & Johrendt, D. Superconductivity at 38 K in the iron arsenide $(Ba_{1-x}K_x)Fe_2As_2$. *Phys. Rev. Lett.* **101,** 107006 (2008).
3. Ni, N. *et al.* Effects of Co substitution on thermodynamic and transport properties and anisotropic H_{c2} in $Ba(Fe_{1-x}Co_x)_2As_2$ single crystals. *Phys. Rev. B* **78,** 214515 (2008).
4. Canfield, P. C., Bud'ko, S. L., Ni, N., Yan, J. Q. & Kracher, A. Decoupling of the superconducting and magnetic (structural) phase transitions in electron-doped $BaFe_2As_2$. *Phys. Rev. B* **80,** 060501 (2009).
5. Pratt, D. K. *et al.* Coexistence of competing antiferromagnetic and superconducting phases in the underdoped $Ba(Fe_{0.953}Co_{0.047})_2As_2$ compound using X-ray and neutron scattering techniques. *Phys. Rev. Lett.* **103,** 087001 (2009).
6. Lester, C. *et al.* Neutron scattering study of the interplay between structure and magnetism in $Ba(Fe_{1-x}Co_x)_2As_2$. *Phys. Rev. B* **79,** 144523 (2009).
7. Lifshitz, I. M. Anomalies of electron characteristics of a metal in the high pressure region. *Sov. Phys. JETP* **11,** 1130–1135 (1960).
8. Liu, G. *et al.* Band-structure reorganization across the magnetic transition in $BaFe_2As_2$ seen via high-resolution angle-resolved photoemission. *Phys. Rev. B* **80,** 134519 (2009).
9. Yang, L. X. *et al.* Electronic structure and unusual exchange splitting in the spin-density-wave state of the $BaFe_2As_2$ parent compound of iron-based superconductors. *Phys. Rev. Lett.* **102,** 107002 (2009).
10. Zhang, Y. *et al.* Unusual doping dependence of the electronic structure and coexistence of spin-density-wave and superconductor phases in single crystalline $Sr_{1-x}K_xFe_2As_2$. *Phys. Rev. Lett.* **102,** 127003 (2009).
11. Hsieh, D. *et al.* Experimental determination of the microscopic origin of magnetism in parent iron pnictides. Preprint at http://arxiv.org/abs/0812.2289 (2008).
12. Kondo, T. *et al.* Unexpected Fermi-surface nesting in the pnictide parent compounds $BaFe_2As_2$ and $CaFe_2As_2$ revealed by angle-resolved photoemission spectroscopy. *Phys. Rev. B* **81,** 060507(R) (2010).
13. Liu, C. *et al.* Three- to two-dimensional transition of the electronic structure in $CaFe_2As_2$: A parent compound for an iron arsenic high-temperature superconductor. *Phys. Rev. Lett.* **102,** 167004 (2009).
14. Yi, M. *et al.* Unconventional electronic reconstruction in undoped $(Ba,Sr)Fe_2As_2$ across the spin density wave transition. *Phys. Rev. B* **80,** 174510 (2009).
15. Zabolotnyy, V. B. *et al.* (π,π) electronic order in iron arsenide superconductors. *Nature* **457,** 569–572 (2009).
16. Zhang, J., Sknepnek, R., Fernandes, R. M. & Schmalian, J. Orbital coupling and superconductivity in the iron pnictides. *Phys. Rev. B* **79,** 220502(R) (2009).
17. Christianson, A. D. *et al.* Static and dynamic magnetism in underdoped superconductor $BaFe_{1.92}Co_{0.08}As_2$. *Phys. Rev. Lett.* **103,** 087002 (2009).
18. Terashima, K. *et al.* Fermi surface nesting induced strong pairing in iron-based superconductors. *Proc. Natl Acad. Sci. USA* **106,** 7330–7333 (2009).
19. Mun, E. D., Bud'ko, S. L., Ni, N. & Canfield, P. C. Thermoelectric power and Hall coefficient measurements on $Ba(Fe_{1-x}T_x)_2As_2$ (T = Co and Cu). *Phys. Rev. B* **80,** 054517 (2009).
20. Fang, L. *et al.* Roles of multiband effects and electron–hole asymmetry in the superconductivity and normal-state properties of $Ba(Fe_{1-x}Co_x)_2As_2$. *Phys. Rev. B* **80,** 140508(R) (2009).
21. Rullier-Albenque, F. *et al.* Hall effect and resistivity study of the magnetic transition, carrier content, and Fermi-liquid behavior in $Ba(Fe_{1-x}Co_x)_2As_2$. *Phys. Rev. Lett.* **103,** 057001 (2009).
22. Ni, N. *et al.* Phase diagrams of $Ba(Fe_{1-x}M_x)_2As_2$ single crystals (M = Rh and Pd). *Phys. Rev. B* **80,** 024511 (2009).
23. Butch, N. P. *et al.* Effective carrier type and field-dependence of the reduced-T_c superconducting state in $SrFe_{2-x}Ni_xAs_2$. *Phys. Rev. B* **81,** 024518 (2010).
24. Evtushinsky, D. V. *et al.* Momentum dependence of the superconducting gap in $Ba_{1-x}K_xFe_2As_2$. *Phys. Rev. B* **79,** 054517 (2009).
25. Park, J. T. *et al.* Electronic phase separation in the slightly underdoped iron pnictide superconductor $Ba_{1-x}K_xFe_2As_2$. *Phys. Rev. Lett.* **102,** 117006 (2009).
26. Fukazawa, H. *et al.* ^{75}As NMR study of hole-doped superconductor $Ba_{1-x}K_xFe_2As_2$ ($T_c \simeq 38$ K). *J. Phys. Soc. Jpn* **78,** 033704 (2009).
27. Fernandes, R. M. *et al.* Unconventional pairing in the iron arsenide superconductors. *Phys. Rev. B* **81,** 140501(R) (2010).
28. Schrieffer, J. R. Wards identity and the suppression of spin fluctuation superconductivity. *J. Low Temp. Phys.* **99,** 397–402 (1995).
29. Parker, D., Vavilov, M. G., Chubukov, A. V. & Mazin, I. I. Coexistence of superconductivity and a spin density wave in pnictide superconductors: Gap symmetry and nodal lines. *Phys. Rev. B* **80,** 100508(R) (2009).

Acknowledgements

We acknowledge Y. S. Kim for his excellent instrumental support at ALS. Ames Laboratory is supported by the Department of Energy—Basic Energy Sciences under Contract No. DE-AC02-07CH11358. ALS is operated by the US DOE under Contract No. DE-AC03-76SF00098.

Author contributions

T.K., C.L. and A.K. devised the concept of the experiments; T.K., C.L., A.K., A.D.P., A.B. and E.R. carried out the ARPES measurements; C.L. analysed the ARPES data with support from T.K. and A.D.P.; R.M.F. and J.S. developed the theoretical model and carried out calculations. N.N., A.N.T., E.D.M., S.L.B. and P.C.C. provided the single crystals and carried out the transport measurements. C.L. prepared the manuscript with support from A.K., P.C.C. and J.S. Section I of the Supplementary Information was prepared by R.M.F. All authors made a substantial contribution.

Additional information

The authors declare no competing financial interests. Supplementary information accompanies this paper on www.nature.com/naturephysics. Reprints and permissions information is available online at http://npg.nature.com/reprintsandpermissions. Correspondence and requests for materials should be addressed to A.K.